

STIM1 over-activation generates a multi-systemic phenotype affecting skeletal muscle, spleen, eye, skin, bones, and the immune system in mice

Roberto Silva-Rojas¹, Susan Treves², Hugues Jacobs^{1,3}, Pascal Kessler¹, Nadia Messaddeq¹, Jocelyn Laporte^{1*}, Johann Böhm^{1*}

¹IGBMC (Institut de Génétique et de Biologie Moléculaire et Cellulaire), Inserm U1258, CNRS UMR7104, Université de Strasbourg, 67404 Illkirch, France

²Departments of Biomedicine and Anaesthesia, Basel University Hospital, Basel University, 4031 Basel, Switzerland

³Institut Clinique de la Souris (ICS), 67404 Illkirch, France

*Correspondence: Johann Böhm (johann@igbmc.fr), Jocelyn Laporte (jocelyn@igbmc.fr)

IGBMC, 1 Rue Laurent Fries, 67404 Illkirch, France

Tel.: +33 (0)3 88 65 34 14

FAX: +33 (0)3 88 65 32 01

Abstract

Strict regulation of Ca^{2+} homeostasis is essential for normal cellular physiology. Store-operated Ca^{2+} entry (SOCE) is a major mechanism controlling basal Ca^{2+} levels and intracellular Ca^{2+} store refilling, and abnormal SOCE severely impacts on human health. Overactive SOCE results in excessive extracellular Ca^{2+} entry due to dominant *STIM1* or *ORAI1* mutations, and has been associated with tubular aggregate myopathy (TAM) and Stormorken syndrome (STRMK). Both disorders are spectra of the same disease and involve muscle weakness, myalgia, and cramps, and additional multi-systemic signs including miosis, bleeding diathesis, hyposplenism, dyslexia, short stature, and ichthyosis. To elucidate the physiological consequences of STIM1 over-activation, we generated a murine model harboring the most common TAM/Stormorken syndrome mutation and characterized the phenotype at the histological, ultrastructural, metabolic, physiological, and functional level. In accordance with the clinical picture of TAM/Stormorken syndrome, the *Stim1*^{R304W/+} mice manifested muscle weakness, thrombocytopenia, skin and eye anomalies, and spleen dysfunction, as well as additional features not yet observed in patients such as abnormal bone architecture and immune system dysregulation. The murine muscles exhibited contraction and relaxation defects as well as dystrophic features, and functional investigations unraveled increased Ca^{2+} influx in myotubes. In conclusion, we provide insight into the pathophysiological effect of the STIM1 R304W mutation in different cells, tissues, and organs, and thereby significantly contribute to a deeper understanding of the pathomechanisms underlying TAM/Stormorken syndrome and other human disorders involving aberrant Ca^{2+} homeostasis and affecting muscle, bones, platelets, or the immune system.

Introduction

Store-operated Ca^{2+} entry (SOCE) is a conserved and ubiquitous mechanism regulating intracellular Ca^{2+} balance, and small disturbances can severely impact on the physiology of various cells, tissues, and organs (1). Ca^{2+} is mainly stored in the endoplasmic/sarcoplasmic reticulum, and its release to the cytosol initiates a plethora of cellular pathways and processes including muscle growth and contraction, T-cell differentiation, or platelet activation. Ca^{2+} store refill relies on the concerted activity of the reticular Ca^{2+} sensor STIM1 and the plasma membrane Ca^{2+} channel ORAI1. STIM1 senses the luminal Ca^{2+} concentration through EF-hands, and Ca^{2+} store depletion induces a conformational change enabling STIM1 oligomerization. The cytosolic domains of the STIM1 oligomers then activate the Ca^{2+} release-activated Ca^{2+} (CRAC) channel ORAI1 to trigger extracellular Ca^{2+} entry (2-4).

Abnormal SOCE has been associated with different human disorders. Recessive *STIM1* and *ORAI1* loss-of-function mutations resulting in insufficient SOCE cause severe immunodeficiency involving recurrent and chronic infections, autoimmunity, ectodermal dysplasia, and muscular hypotonia (OMIM #612782 and 612783) (1, 5, 6). In contrast, dominant *STIM1* and *ORAI1* gain-of-function mutations inducing excessive Ca^{2+} entry through SOCE over-activation were found in patients with tubular aggregate myopathy (TAM, OMIM #160565 and #615883) and Stormorken syndrome (STRMK, OMIM #185070) (7-10). Both conditions are part of a clinical continuum and are characterized by progressive muscle weakness, cramps, and myalgia (11), and additional multi-systemic signs including thrombocytopenia, hyposplenism, miosis, ichthyosis, short stature, hypocalcemia, and dyslexia (12-18). Age of onset, disease severity, and occurrence of non-muscle features are heterogeneous and generally correlate with the genotype. The most common gain-of-function mutation R304W, affecting a conserved amino acid in the cytosolic domain of STIM1, was found in twelve unrelated families essentially presenting with the full multi-

systemic picture constituting the diagnosis of Stormorken syndrome (8-10, 14, 19, 20). Functional studies demonstrated that the R304W mutation induces a helical elongation of the cytosolic domain of STIM1 and thereby promotes the exposure of the ORAI1-interacting SOAR domain, resulting in constitutive ORAI1 channel activation (21). Moreover, electrophysiological studies have shown that the R304W mutation suppresses fast Ca^{2+} -dependent channel inactivation (CDI) of ORAI1, suggesting that R304W also entails prolonged Ca^{2+} influx (10).

Mammalian models with abnormal SOCE are rare, impeding a detailed analysis of the long-term consequences of abnormal Ca^{2+} homeostasis on the entire organism and in different tissues, and precluding functional investigations on the sequence of events leading to the multi-systemic aberrations observed in severe combined immunodeficiency or TAM/Stormorken syndrome. *Stim1*^{-/-} and *Orai1*^{-/-} mice showed high neonatal lethality, and surviving animals manifested low body weight and significant hypotonia leading to death within a few weeks (22-24). A similar phenotype was observed for *Orai1*^{R93W/R93W} knock-in mice expressing a non-functional Ca^{2+} channel (25). Tissue-specific knockout of *Stim1* demonstrated a decrease in number and function of T cells (26) and a reduced ability of platelets to switch from a pro-adhesive to a pro-coagulant state (27), but provided only a narrow view on the physiological consequences of SOCE suppression. The *Stim1*^{Sax} mouse, generated through random mutagenesis and harboring the same D84G mutation as in a single family with tubular aggregate myopathy (7), displayed spleen enlargement and increased basal Ca^{2+} levels in the platelets resulting in a pre-activation state and elevated platelet consumption (28). However, a potential phenotype of muscle, skin, or bones was not evaluated.

In order to shed light on the multi-systemic features of TAM/Stormorken syndrome, we generated a targeted knock-in mouse model harboring the most common *STIM1* gain-of-

function mutation R304W. Our exhaustive phenotypic characterization revealed that the *Stim1*^{R304W/+} mice recapitulate the main clinical features observed in TAM/Stormorken patients including muscle weakness, thrombocytopenia, skin and eye anomalies, and spleen dysfunction. We also detected increased glucose tolerance, abnormal bone architecture, and abnormal immune cell counts, which all might have escaped diagnosis in TAM/Stormorken syndrome patients to date. Overall, this study highlights the relevance of SOCE in several tissues and organs in normal and pathological conditions, and describes a new mouse model as a valuable tool to study the physiopathology and possible therapeutic approaches for TAM/Stormorken syndrome, as well as for other Ca²⁺-related disorders involving aberrations of muscle, bones, platelets, or the immune system.

Results

To address the physiological impact of SOCE over-activation, we generated a mouse model carrying the most recurrent *STIM1* gain-of-function mutation found in patients with TAM/Stormorken syndrome (8-10). The c.910A>T (p.R304W) point mutation was introduced by homologous recombination targeting exon 7 of *Stim1* in C57BL/6N mouse embryonic stem cells (ESCs) to generate heterozygous *Stim1*^{R304W/+} and homozygous *Stim1*^{R304W/R304W} mice (Supplemental Figures S1A and S1B).

Viable homozygous *Stim1*^{R304W/R304W} mice were not obtained at genotyping 3 days after birth, and in breeding cages containing *Stim1*^{+/+} (WT) and *Stim1*^{R304W/+} animals, the statistically significant offspring ratio was 59% *Stim1*^{+/+} and 41% *Stim1*^{R304W/+}. The absence of homozygous *Stim1*^{R304W/R304W} mice and the decreased birth rate of heterozygous *Stim1*^{R304W/+} animals suggests that the STIM1 R304W mutation causes embryonic or perinatal lethality especially in the homozygous state. The point mutation however did not significantly alter the

STIM1 protein level in muscle, as it was comparable in WT and *Stim1*^{R304W/+} tibialis anterior (TA), soleus, and gastrocnemius muscles (Supplemental Figure S1C).

The *Stim1*^{R304W/+} animals underwent thorough phenotypic examinations to investigate the multi-systemic signs and symptoms of TAM/Stormorken syndrome patients and to potentially uncover anomalies not reported in patients yet. Importantly, the *Stim1*^{R304W/+} mice had a reduced life span with only half of the *Stim1*^{R304W/+} males and females living longer than 9 months (Figure 1A). Functional and morphological investigations were therefore carried out at 4 months and 9 months to assess disease development.

Stim1^{R304W/+} mice are smaller and manifest spleen enlargement

Tracking of body weight and length revealed that the *Stim1*^{R304W/+} mice were smaller and lighter than the WT littermates. At 4 months of age, the body weight was reduced by 21.3% in *Stim1*^{R304W/+} males and by 11.9% in *Stim1*^{R304W/+} females (Figure 1B), and body length was reduced by 7.7% in *Stim1*^{R304W/+} males and by 7.2% in *Stim1*^{R304W/+} females (Figure 1C). Accordingly, patients with TAM/Stormorken syndrome and STIM1 R304W mutation were described with a shorter stature (8, 9, 29). Using quantitative nuclear magnetic resonance (qNMR), we also detected a decreased lean and fat mass rate in *Stim1*^{R304W/+} compared to WT mice, especially in males (Supplemental Figure S2). To investigate whether the delayed growth results from bone anomalies, we assessed the morphology of the 5th lumbar vertebra, the distal femur, and the midshaft tibia by micro-CT. We detected a decreased cellular density, a reduced bone marrow area, and abnormal mechanical properties with a 10% decrease of polar moment of inertia (MOI), indicating a reduced strength and stiffness of the bones of *Stim1*^{R304W/+} mice. (Figure 1D and Supplemental Tables S1-S3).

We next weighed various organs, and in agreement with the reduced body size, *Stim1*^{R304W/+} heart, brain, and liver were slightly smaller and lighter or similar compared to WT

littermates. We noted a significant spleen enlargement in *Stim1*^{R304W/+} mice with an increase in spleen weight of 55% in *Stim1*^{R304W/+} females and 31% in *Stim1*^{R304W/+} males as compared to wild-type controls (Figure 1E). The analysis of different lower limb muscles revealed specific weight discrepancies. While the tibialis anterior and extensor digitorum longus (EDL) were comparable in *Stim1*^{R304W/+} and WT littermates, the *Stim1*^{R304W/+} gastrocnemius was hypotrophic with a 36.6% weight reduction in *Stim1*^{R304W/+} females and a 19.3% reduction in *Stim1*^{R304W/+} males, while the soleus was hypertrophic with an increased weight of 57.3% in *Stim1*^{R304W/+} females and 58.4% in *Stim1*^{R304W/+} males (Figure 1F).

Stim1^{R304W/+} mice manifest upward gaze paresis, thrombocytopenia, and skin anomalies

We assessed a potential eye phenotype in *Stim1*^{R304W/+} mice using a slit lamp. Although a miosis was not apparent, we noted an upward gaze paresis (Figure 1G), a limitation of eye movement described in TAM/Stormorken syndrome patients (7, 14). Both *Stim1*^{R304W/+} males and females manifested prolonged bleeding times, and blood counts showed a marked reduction of platelets of 78% in *Stim1*^{R304W/+} females and 79% in *Stim1*^{R304W/+} males compared to control littermates (Figure 1H). The platelets were significantly bigger in the knock-in animals with an increase of mean platelet volume of 63% in *Stim1*^{R304W/+} females and 74.4% in *Stim1*^{R304W/+} males. Bleeding diathesis is also commonly seen in TAM/Stormorken syndrome patients, and was shown to result from abnormal platelet structure and function (8, 9, 14, 19).

Patients with TAM/Stormorken syndrome also often manifest ichthyosis (8, 9, 19), and accordingly we observed skin irritations in *Stim1*^{R304W/+} mice. Histological skin analyses revealed an enlarged dermis and a reduced fat layer compared to the wild-type controls, conforming the qNMR data showing a decreased lean and fat mass rate in *Stim1*^{R304W/+} mice

(Supplemental Figure S3), and potentially corresponding to the skin phenotype in TAM/Stormorken syndrome patients and mice.

The $Stim1^{R304W/+}$ mice manifest abnormal immune cell counts

SOCE plays a pivotal role in the proliferation and activation of T and B cells, and suppressed Ca^{2+} entry resulting from *STIM1* or *ORAI1* loss-of-function mutations has been associated with life-threatening immunodeficiency (5, 6).

To investigate the impact of the STIM1 R304W mutation on the immune system, we quantified the hematopoietic cells in the blood and detected increased numbers of neutrophils and monocytes and decreased numbers of total lymphocytes in $Stim1^{R304W/+}$ mice compared to WT littermates (Figure 2A and 2B), and we obtained similar results in spleen (Supplemental Figure S4). Histological investigations on $Stim1^{R304W/+}$ spleen revealed megakaryocyte hyperplasia (Figure 2C). Of note, further analyses uncovered a significant reduction of regulatory T cells and natural killer cells in $Stim1^{R304W/+}$ spleen (Figure 2D and Supplemental Figure S4). Regulatory T cells modulate the immune system and maintain the tolerance to self-antigens to prevent auto-immune disorders. Our findings of regulatory T cell reduction might therefore indicated an over-active immune system in $Stim1^{R304W/+}$ mice.

$Stim1^{R304W/+}$ mice exhibit reduced muscle force and delayed muscle relaxation

In the open field test, especially the $Stim1^{R304W/+}$ females covered less distance and moved with lower pace compared to WT littermates (Figure 3A). To assess whether this difference results from impaired coordination or abnormal muscle force or fatigue, we performed a series of physiological tests.

Both $Stim1^{R304W/+}$ and WT littermates performed similarly on the rotarod, indicating that balance, motor coordination, and the ability for short-duration exercise are not significantly altered in knock-in animals (Figure 3B). Plethysmography essentially revealed comparable

breathing values between *Stim1*^{R304W/+} and WT littermates with exception of an enhanced pause suggesting partial bronchial obstruction in the knock-in animals (Supplemental Table S4). However, grip strength and hanging time were significantly reduced in *Stim1*^{R304W/+} mice (Figure 3C-D). Compared to the WT littermates, the 4-paw grip strength was reduced by 18.7% in female *Stim1*^{R304W/+} mice, and by 27.3% in male *Stim1*^{R304W/+} mice. The majority of WT mice successfully accomplished the 60 s hanging test, and all sustained for at least 46 s. In contrast, female *Stim1*^{R304W/+} mice fell after 20 s in average, and male *Stim1*^{R304W/+} mice after 17 s, which corresponds to a reduction of hanging time of 64.4% and 70.8%, respectively.

To further investigate the muscle phenotype, we quantified the *in situ* muscle force and resistance to fatigue of the tibialis anterior from 9 months old *Stim1*^{R304W/+} mice using the Aurora force transducer. Following sciatic nerve stimulation, especially *Stim1*^{R304W/+} males manifested a significantly reduced maximal and specific force compared to WT littermates. While WT mice developed an average specific force of 14.7 mN/mg, female *Stim1*^{R304W/+} mice reached 14.3 mN/mg, and male *Stim1*^{R304W/+} mice 11.3 mN/mg (- 23.7%) (Figure 3E). We obtained similar results by direct stimulation of the muscle, demonstrating that the nerve-to-muscle signal transmission is not altered (Supplemental Figure S5).

Noteworthy, we observed a shift in muscle relaxation subsequent to stimulation in *Stim1*^{R304W/+} compared to WT tibialis anterior (Figure 3E). We therefore applied a continuous stimulation of the sciatic nerve and quantified the decrease of force over time (Figure 3F). We observed that the specific force of WT mice drops to 50% after 11.6 s in average, and after 17.7 s in case of *Stim1*^{R304W/+} mice, representing an increased time to fatigue. We also noted that the *Stim1*^{R304W/+} mice developed maximal specific force at lower stimulation frequencies compared to WT mice (Supplemental Figure S6). Taken together, our force transducer experiments revealed that *Stim1*^{R304W/+} tibialis anterior contracted at lower

stimulation frequencies, produced less force at higher stimulation frequencies, and relaxed with delay in comparison with WT controls, demonstrating that the STIM1 R304W mutation affects both muscle contraction and muscle relaxation.

Stim1^{R304W/+} mice do not show tubular aggregates in muscle fibers

Tubular aggregates represent the main histopathological hallmark in skeletal muscle from TAM/Stormorken syndrome patients. These central or subsarcolemmal basophilic accumulations appear in red on modified Gomori trichrome staining, and in dark blue on nicotinamide adenine dinucleotide-tetrazolium reductase (NADH-TR) staining especially in fast-twitch type II fibers (11, 30). Additional features as fiber size variability, internalized nuclei, endomysial fibrosis, type I fiber predominance, and type II fiber atrophy are consistently seen as well (7, 12, 13, 15, 16, 19, 31-33).

Histological analyses of tibialis anterior sections from *Stim1^{R304W/+}* mice at 4 months and 9 months, and of EDL, soleus, and gastrocnemius muscles at 4 months revealed a 4 to 8 fold increase of internalized nuclei, fibrosis, and infiltration of inflammatory cells, but tubular aggregates were not detected (Figure 4A, Supplemental Figures S7-S12). We also noticed an altered fiber type composition with an increased ratio of slow-twitch type I fibers in all analyzed muscles. To investigate fiber size, we measured the MinFerret diameter and uncovered a slight reduction in *Stim1^{R304W/+}* TA fiber caliber in males compared to WT littermates at 4 months of age (Figure 4B), while no difference was seen in females (Supplemental Figure S13A). We also noted a subset of fibers with abnormal shape on the *Stim1^{R304W/+}* tibialis anterior, EDL, soleus, gastrocnemius muscle sections, and circularity measurements on TA sections confirmed a tendency of increased rounded fibers in both male and female *Stim1^{R304W/+}* mice (Figure 4C, Supplemental Figure S13B). Alizarin red staining

demonstrated that the 4-7% of rounded fibers contain high amounts of Ca^{2+} (Figure 4A and Supplemental Figures S7 and S9-11), indicating that these fibers are damaged.

Ultrastructural analyses on transversal and longitudinal *Stim1*^{R304W/+} tibialis anterior sections uncovered swollen mitochondria at both 4 and 9 months of age in largely intact muscle fibers, and confirmed the absence of tubular aggregates (Figure 4D and Supplemental Figure S14).

Stim1^{R304W/+} mice manifest blood hypocalcemia and increased Ca^{2+} influx in skeletal muscle

In view of the abnormal contraction and relaxation properties of *Stim1*^{R304W/+} muscle, and the histological findings of fibers with elevated Ca^{2+} content, we next focused on the Ca^{2+} level in blood and skeletal muscle. This is of particular importance, as TAM/Stormorken syndrome patients were commonly reported with blood hypocalcemia (8-10, 12, 13, 15, 19), and functional investigations demonstrated that the *STIM1* gain-of-function mutations induce excessive Ca^{2+} entry in patient myoblasts through SOCE over-activation (7, 16).

We measured decreased Ca^{2+} levels and consequently increased phosphate levels in the blood from *Stim1*^{R304W/+} mice (Figure 5A). We also detected a 6 to 8 fold increase of serum creatine kinase (CK) (Supplemental Figure S15), residing within the range of typical CK elevation in TAM/Stormorken syndrome patients (7, 9, 12). In addition, we found altered hepatic enzyme activities (Supplemental Figure S16A), and increased insulin and decreased glucose levels in accordance with increased glucose tolerance (Supplemental Figures S16B and S16C). It has recently been demonstrated that inhibition of SOCE has an adverse effect and results in impaired insulin secretion from pancreatic islets and systemic glucose intolerance (34, 35). Together with our data, it illustrates that tight Ca^{2+} regulation is essential for β -cell function and that abnormal SOCE directly impacts on insulin secretion and the glucose level in blood.

We next assessed Ca^{2+} homeostasis in cultured myotubes obtained by differentiation of myoblasts from *Stim1*^{R304W/+} and WT mice. At physiological 2 mM Ca^{2+} conditions in the

medium, the *Stim1*^{R304W/+} myotubes exhibited increased resting Ca²⁺ levels compared to WT myotubes (Figure 5B). In a second experiment, we kept the myotubes in Ca²⁺-free media, and administration of 10 mM Ca²⁺ to the medium induced a significantly more pronounced Ca²⁺ influx in myotubes from *Stim1*^{R304W/+} as compared to the control (Figure 5C-D). Using a combination of caffeine and thapsigargin to maximally deplete the Ca²⁺ stores, we found that the Ca²⁺ content in the reticulum was comparable in WT and *Stim1*^{R304W/+} myotubes (supplemental Figure S17). Taken together, the *Stim1*^{R304W/+} myotubes exhibited increased resting Ca²⁺ levels and increased extracellular Ca²⁺ influx, while Ca²⁺ storage was not affected.

To investigate the downstream effects of excessive Ca²⁺ influx, we scaled the expression of the SOCE genes *Stim1* and *Orail1*, as well as of *Casq1* and selected skeletal muscle genes regulated by the Ca²⁺-dependent transcription factor NFAT. Quantitative RT-qPCR on tibialis anterior from *Stim1*^{R304W/+} mice revealed a downregulation of *Stim1* in males but not in females, of *Nfatc1* and *Nfatc3*, and an upregulation of the myogenic differentiation markers *Myog* and *Myf5* (Figure 4E). We also noted a reduced expression of *Casq1* in *Stim1*^{R304W/+} tibialis anterior. *Casq1* is however specifically expressed in type II fibers, and the abnormal composition of the *Stim1*^{R304W/+} tibialis anterior with an increased ratio of type I fibers most probably accounts for the seemingly downregulation of *Casq1*.

Overall, these data demonstrate that the STIM1 R304W mutation induces excessive Ca²⁺ influx in skeletal muscle, and leads to partial muscle fiber degeneration involving elevated serum CK levels and the upregulation of muscle differentiation factors, conforming to the dystrophic features observed on muscle sections.

Discussion

Ca²⁺ serves as a second messenger in a variety of biological processes in both excitable and non-excitable cells. Store-operated Ca²⁺ entry (SOCE) is a primary mechanism regulating extracellular Ca²⁺ entry, and abnormal SOCE leads to severe human disorders. Insufficient SOCE resulting from *STIM1* or *ORAI1* loss-of-function causes immunodeficiency, while overactive SOCE resulting from *STIM1* or *ORAI1* gain-of-function causes TAM/Stormorken syndrome (1). To elucidate the physiological effect of STIM1 over-activation, we generated a mouse model harboring the most common STIM1 gain-of-function mutation R304W. The *Stim1*^{R304W/+} mice phenotypically mimicked TAM/Stormorken syndrome, and we also discovered additional characteristics of high medical importance that have not been reported for TAM/Stormorken syndrome patients yet. With a main focus on skeletal muscle, our in-depth investigations on the *Stim1*^{R304W/+} mouse provides a first insight into the pathomechanisms resulting from SOCE over-activation and leading to Ca²⁺-related physiological dysfunction.

The Stim1^{R304W/+} mouse as a tool to study TAM/Stormorken syndrome and SOCE over-activation

Tubular aggregate myopathy and Stormorken syndrome are clinically overlapping multi-systemic disorders characterized by tubular aggregate myopathy, miosis, thrombocytopenia, hyposplenism, short stature, ichthyosis, and dyslexia (29). In agreement with the clinical presentation of TAM/Stormorken syndrome patients, the *Stim1*^{R304W/+} mice were smaller than the control littermates, and manifested muscle weakness, thrombocytopenia, spleen dysplasia, and skin irritations, demonstrating that our mouse model is a suitable and valuable tool to study the physiopathology and the disease development of TAM/Stormorken syndrome. In line with the reported Ca²⁺ overload and excessive Ca²⁺ influx in myoblasts and myotubes from TAM/Stormorken syndrome patients (7, 16), we measured hypocalcemia in the blood and elevated resting Ca²⁺ levels in *Stim1*^{R304W/+} myotubes, as well as SOCE over-activation

and excessive extracellular Ca^{2+} entry without prior Ca^{2+} store depletion. This confirms that the muscle dysfunction and most probably also the multi-systemic aberrations of TAM/Stormorken syndrome are a direct consequence of abnormal Ca^{2+} homeostasis, and demonstrates that our *Stim1*^{R304W/+} mouse can serve as a model to investigate the consequences and treatment options of overactive SOCE in Ca^{2+} -related disorders.

Impact of SOCE over-activation on muscle contraction and relaxation

The STIM1 R304W mutation was previously shown to induce excessive extracellular Ca^{2+} entry through a dual pathogenic effect: it induces constitutive STIM1 and SOCE activation and suppresses fast inactivation of the ORAI1 Ca^{2+} entry channel (10, 21). Accordingly, we observed higher resting Ca^{2+} levels as well as excessive extracellular Ca^{2+} entry despite replete Ca^{2+} stores in myotubes from *Stim1*^{R304W/+} mice. In resting skeletal muscle, cytosolic Ca^{2+} concentrations are low and vary between 30 and 60 nM depending on the fiber type (36), and small Ca^{2+} level changes induce major physiological processes. Ca^{2+} release from the sarcoplasmic reticulum triggers muscle contraction and the generation of force, repeated contractions require the maintenance of high Ca^{2+} gradients and the strict regulation of luminal and cytosolic Ca^{2+} balance, and muscle relaxation occurs when Ca^{2+} is removed from the contractile unit (37). The *Stim1*^{R304W/+} mice manifested reduced muscle force as well as abnormal muscle contraction and relaxation, all three presumably resulting from aberrant Ca^{2+} homeostasis. The elevated resting cytosolic Ca^{2+} levels in *Stim1*^{R304W/+} muscle provoked rapid fiber contraction, diminished the effect of high stimulation frequencies on force production, and also extended the relaxation time. The delayed muscle relaxation might thereby explain the muscle cramping phenotype observed in a large number of TAM/Stormorken syndrome patients (8, 10-13, 17, 19, 31, 38). The high resting Ca^{2+} levels most probably also account for the swollen mitochondria and the dystrophic features observed in *Stim1*^{R304W/+} muscle. Histological analyses revealed rounded and Ca^{2+} -rich fibers,

typically seen to a larger extent in dystrophies involving major fiber degeneration and regeneration (39). Accordingly, we observed a subset of regenerating fibers in *Stim1*^{R304W/+} muscle, increased expression of the myogenic regulators factors *Myf5* and *Myog* (40), as well as 6 to 8 fold increased serum creatine kinase levels, demonstrating intensified muscle fiber degeneration and myogenesis in *Stim1*^{R304W/+} mice.

The role of tubular aggregates in disease development

Histological analyses of muscle biopsies from TAM/Stormorken syndrome patients typically show basophilic accumulations in the muscle fibers appearing in red on modified Gomori trichrome staining, and corresponding to densely packed membrane tubules (7-11). Tubular aggregates also naturally accumulate in normal murine muscle with age, and can especially be seen in type II fibers from 10 months in most laboratory mice strains (41).

Surprisingly, analyses of different muscles failed to detect tubular aggregates in the *Stim1*^{R304W/+} mice at different time points and up to 9 months. Given the explicit and multi-systemic TAM/Stormorken syndrome phenotype developed by *Stim1*^{R304W/+} mice, we conclude that physiological differences between humans and mice most probably account for the presence or absence of tubular aggregates in pathologic skeletal muscle, and that tubular aggregate formation and disease-related muscle dysfunction are not causally linked. This of particular importance for potential therapeutic approaches, as tubular aggregates do not represent suitable therapeutic targets, and cannot serve as readouts to assess treatment efficacy.

It is conceivable that the abundant tubular aggregates in the muscle fibers of TAM/Stormorken syndrome patients do not impair muscle function, but rather exert a protective role and prevent fiber degeneration by trapping excessive Ca^{2+} . In compliance,

signs of dystrophic-like fiber degeneration are more prominent in muscle from *Stim1*^{R304W/+} mice compared to muscle from TAM/Stormorken syndrome patients.

Impact of the STIM1 R304W mutation on coagulation and the immune system

The bleeding diathesis observed in many TAM/Stormorken patients results from abnormal platelet number, structure and function. It could be shown that the TAM/Stormorken syndrome platelets display increased basal Ca²⁺ levels prior to activation, leading to diminished response to stimulation and reduced platelet-platelet adhesion (8, 9, 14, 19). Thrombocytopenia with a reduced platelet number resulting in prolonged bleeding times was also seen in our *Stim1*^{R304W/+} mice. We additionally observed an increased mean platelet volume, considered as a marker for diverse inflammatory diseases (42-44).

The immune system provides protection against various disease-causing pathogens and is based on a complex interplay between different effector cells with specialized function. T helper 17 cells (Th17) are pro-inflammatory cells recruiting neutrophils to the sites of infection, whereas regulatory T cells (Treg) have an antagonistic effect and inhibit immune response. The balance between Th17 and Treg cells is therefore critical for the development of autoimmune and inflammatory diseases (45). The *Stim1*^{R304W/+} mice displayed a significant reduction of Treg cells and a simultaneous upregulation of neutrophils and monocytes, suggesting an imbalance of Th17 and Treg, promoting the maintenance of inflammation. Indeed, the *Stim1*^{R304W/+} mice showed multiple signs of inflammation as infiltration of inflammatory cells in muscle, increased mean platelet volume, spleen hyperplasia, bronchial obstruction, and an enlarged dermis. Ichthyosis has often been described in TAM/Stormorken syndrome patients (8, 9, 19), but detailed investigations on skin biopsies have not been performed. The *Stim1*^{R304W/+} mice manifested a skin phenotype as well, and our findings point to an underlying inflammatory disease causing the urticarial eruptions. Noteworthy, the

Stim1^{Sax} mouse, harboring another *Stim1* gain-of function mutation, similarly displayed spleen enlargement and increased platelet size (28), and additional signs of inflammation might be more discreet due to the milder mutational effect of the *Stim1* D84G mutation compared to R304W.

Impact of the STIM1 R304W mutation on growth and lifespan

Here we show that the *Stim1^{R304W/+}* mice manifest an abnormal architecture of cortical and trabecular bones, resulting in diminished mechanical properties and bone strength. It has previously been reported that mice lacking ORAI1 are smaller than control littermates, which partially results from deficient bone development (46, 47). It could be demonstrated that impaired SOCE in precursor cells of both osteoblasts and osteoclasts leads to reduced differentiation and consequently to decreased bone density (46, 47). This suggests that normal bone physiology strongly depends on strict SOCE regulation, and that bone anomalies resulting from insufficient or overactive SOCE compromise bone stability and growth.

A striking feature of the *Stim1^{R304W/+}* mouse is the reduced life span. We did not observe any correlation between the overall health status or the physical performances of the *Stim1^{R304W/+}* mice and the time of death, and we didn't note specific behavioral anomalies preceding death. The discrepancy in body weight and size, and in motor performances between WT and *Stim1^{R304W/+}* mice increases with time, and only 50% of the *Stim1^{R304W/+}* mice live longer than 9 months. We also detected spleen and bone anomalies, indications for an inflammatory disease, and we found evidences for abnormal hepatic function and glucose metabolism. The totality of these signs might reflect an accelerated ageing process or might be the result of multi-organ deterioration due to continuous Ca^{2+} stress. Premature mortality and a subset of the multi-systemic murine phenotypes including bone, metabolic, or immune system anomalies have not been reported for TAM/Stormorken patients yet, but may currently be

unrecognized due to the recent discovery of the causative genes and the respective possibilities of molecular diagnosis. Regular clinical examinations and an extended follow-up of multiple organs and tissues is therefore of major medical importance for TAM/Stormorken syndrome patients.

SOCE insufficiency and over-activation cause mirror diseases

STIM1 and *ORAI1* mutations have been associated with different human disorders depending on the mutational impact and the mode of inheritance. Recessive *STIM1* and *ORAI1* loss-of-function mutations induce severe immunodeficiency characterized by early-onset and recurrent infections, autoimmunity, muscular hypotonia, and ectodermal dysplasia (1). Functional investigation demonstrated that the mutations abolished SOCE either through *STIM1* or *ORAI1* loss, impaired *STIM1*-*ORAI1* interaction, or through *ORAI1* channel impermeability, and the profound inhibition of Ca^{2+} influx in T cell, B cells, and myofibers are the primary cause of the immune system and muscle dysfunction observed in the patients (5, 6, 48-53). By contrast, dominant *STIM1* and *ORAI1* gain-of-function mutations induce TAM/Stormorken syndrome, and SOCE over-activation is presumably responsible for the multi-systemic phenotype encompassing muscle weakness, miosis, thrombocytopenia, hyposplenism, ichthyosis short stature, and dyslexia (7-10, 12-14, 17, 19).

Despite the opposite mutational impact, SOCE insufficiency or SOCE over-activation involving Ca^{2+} imbalance can have a similar effect on different tissues as shown by platelet dysfunction and prolonged bleeding times, muscle weakness, reduction of regulatory T cells, and abnormal bone architecture in *Stim1*^{-/-} (23), *Orai1*^{-/-} (46, 47) or *Stim1*^{R304W/+} mice (this study).

Concluding remark

In conclusion, the present study significantly contributes to a better understanding of the pathomechanisms leading to TAM/Stormorken syndrome and our mouse model proved to be a valuable tool to investigate the pathophysiological consequences of SOCE over-activation and aberrant Ca^{2+} homeostasis in various cells, tissues, and organs, associated with a plurality of rare and common human disorders.

Materials and Methods

Animal care and generation of the $\text{Stim1}^{R304W/+}$ mouse model

Animal care and experimentation was in accordance with French and European legislation and approved by the institutional ethics committee (project numbers 2016031110589922, 2016040511578546, 2017092717177977). Mice were housed in ventilated cages with free access to food and water in temperature-controlled rooms with 12 hours day light/dark cycles.

The $\text{Stim1}^{R304W/+}$ (Stim1^{tm3lcs}) mutant mouse line was established at the ICS (Institut Clinique de la Souris; <http://www.ics-mci.fr/en/>). In brief, C57BL/6N mouse embryonic stem (ES) cells were electroporated with a targeting vector carrying the A>T transversion at cDNA position 910 (NM_009287.5) and a floxed neomycin resistance cassette with an auto-excision transgene. Following G418 selection, the clones were analyzed by long-range PCR and Southern blot using an internal neomycin probe and an external 5' probe. The selected ES clone was karyotyped and micro-injected into BALB/C blastocysts. Resulting male chimeras were bred with WT C57BL/6N females, and germline transmission with direct excision of the selection cassette was achieved in the first litter. Genotyping was performed with following primers: GCAGGTAGGAGAGTGTACAGGATGCCTT (forward, Ef) and CTTTCCATCCCCACTGCCATTTT (reverse, Er). Sequencing primers were CAGGAGGAGCACCGAACTGTGGAA (forward, Mf) and TTACGCACCGCCCAAGGCAT (reverse, Nr).

Open field, rotarod, grip test, hanging test

The open fields (Panlab, Barcelona, Spain) were placed in a homogeneously illuminated room and virtually divided into central and peripheral areas. Each mouse was placed in the periphery and allowed to freely explore the field for 20 min, with the experimenter out of the animal's sight. The covered distance and the average speed of moving were recorded.

The coordination of the animals was measured using a Rotarod apparatus (Bioseb, Vitrolles, France) with an accelerating scale from 4 to 40 rpm. The 4 paw grip strength was assessed with a dynamometer (Bioseb), and for the hanging test, mice were suspended on a cage lid for up to 60 s and the time to fall was recorded.

Pupillary reflex and pupil imaging

The pupillary light reflex was examined on restrained mice using a SL990 slit lamp biomicroscope (CSO, Florence, Italy) at 16x magnification using broad beam illumination, and varied back and forth from the minimal to the highest intensity setting. For pupil imaging, mice were anesthetized with isoflurane (2% in a 50/50 mix of air and O₂ at 0.4 ml/min), the corneas were covered with a carbomere ophthalmic gel (TVM, Lempdes, France), and imaged with a Micron III camera equipped with the mouse lens (Phoenix Research Laboratories, Pleasanton, USA).

qNMR and bone morphology

Whole body composition of fat content, lean tissues, and free body fluid was assessed with a Minispec+ analyzer (Bruker, Billerica, USA) by Nuclear Magnetic Resonance (NMR) during light period on conscious fed mice.

Bone morphology was assessed on the 5th lumbar vertebra, the distal femur and midshaft tibia using the Quantum micro-CT scanner (Perkin Elmer, Waltham, USA). All scans were

performed with an isotropic voxel size of 10 μm , 160 μA tube current, and 90 kV tube voltage. Gray scale images were pre-processed using the ImageJ software, and morphological 3D measurements were further performed using the CTAn software (Bruker). For the 5th lumbar vertebra and the distal femur, the analysis included bone volume fraction, and trabecular thickness, number, and separation. For the tibia midshaft, the analysis included measures of cortical thickness, bone area fraction, total area, bone area, marrow area and polar moment of inertia. Representative images were created by using the CTvol software (Bruker).

Metabolic studies and blood counts

Blood chemistry was assessed following retro-orbital puncture under isoflurane anesthesia to determine glucose, Ca^{2+} , phosphor (P), transaminases (ASAT, ALAT), creatine kinase (CK) and alkaline phosphatase (ALP) levels using the OLYMPUS AU-400 automated laboratory work station (Beckmann Coulter, Brea, USA) with kits and controls supplied by Beckmann Coulter, Wako Chemical Inc (Richmond, USA), or Randox Laboratories (Crumlin, UK). Insulin was measured on a BioPlex analyser (BioRad, Hercules, USA) using the Mouse Metabolic Magnetic bead panel kit (Merck, Darmstadt, Germany). Blood counts were performed on the ADVIA 120 system (Siemens, Munich, Germany).

To assess glucose tolerance, glucose was administered by intraperitoneal injection, and blood glucose levels were measured at different time points over 120 min during the light period, and after overnight fasting using the Accu-Chek (Roche Diagnostics, Basel, Switzerland).

Immunology

Mouse spleens were collected in 1 mL sample collection buffer, transferred to a GentleMACS C tube (Miltenyi Biotec, Bergisch Gladbach, Germany) containing enzyme

cocktail mix, and dissociated with the GentleMACS tissue dissociator (Miltenyi Biotec). Cell suspensions were filtered and diluted 1:100 in Sytox green solution (ThermoFisher Scientific, Waltham, USA), and run on an ATTUNE NxT Flow Cytometer® (ThermoFisher Scientific) with 4×10^6 cells per sample and well. Red blood cells were lysed in 30 μ L 1x RBC lysis buffer for 1 min at RT, and the reaction was stopped with 250 μ L FACS buffer. Fc receptors were then blocked with 100 μ L 2.4G2 serum. IMPC1 and IMPC2 Immunostaining was performed in 100 μ L antibody cocktails and incubated in the dark for 20 min at 4°C. Finally, cell pellets were resuspended in 250 μ L HBSS/2% (v/v) FCS with Sytox blue solution (ThermoFisher Scientific) for exclusion of dead cells. Samples were acquired on a SORP® BD LSR2 FORTRESSA (BD Biosciences, Franklin Lakes, USA), data were compensated with BD FACS DIVA 8.0.1 software (BD Biosciences), and FCS files were run on R using Flowdensity package for automated supervised gating. Frequencies of populations were calculated as defined in <https://www.mousephenotype.org/impress/protocol/174/7>. Results per panel were visualized as fold change on a radar plot, frequencies were transformed in asinh, and run on the TMEV software for PCA analysis, hierarchical clustering (Euclidian distance, centered linkage) or statistical tests (ANOVA).

In vivo muscle force and fatigue

The tibialis anterior is well characterized and suitable for force measurements, and the TA contraction properties were assessed *in situ* using the Complete1300A Mouse Test System (Aurora Scientific, Aurora, Canada). Mice were anesthetized through intraperitoneal injection of domitor/fentanyl mix (2/0.28 mg/Kg), diazepam (8 mg/Kg) and domitor (0.28 mg/Kg). Knees and feet were fixed, and the distal tendon of the tibialis anterior was excised and attached to the isometric transducer. The sciatic nerve or the muscle were stimulated by pulses of 1-125 Hz to measure maximal force. The specific force corresponds to the maximal

force divided by the tibialis anterior weight. Following a rest period of 5 min, sciatic nerve or muscle were then stimulated at 50 Hz for 20 s and the time corresponding to a force decrease of 50% was recorded as the time to fatigue.

Histology and electron microscopy

Spleen and skin were fixed in formaldehyde and embedded in paraffin, and 5 μm sections were stained with hematoxylin and eosin (H&E) using routine protocols to assess histological anomalies. Tibialis anterior, EDL, soleus, and gastrocnemius muscles were frozen in liquid nitrogen-cooled isopentane, and 8 μm sections were stained with H&E, ATPase (pH 4.3), modified Gomori trichrome, and Alizarin red to assess muscle fiber morphology and typing, nuclear positioning, presence of tubular aggregates, and Ca^{2+} deposits using the Nanozoomer 2HT slide scanner (Hamamatsu, Japan).

Fiber MinFerret distribution and circularity were determined on 8 μm tibialis anterior sections stained with Hoechst (Sigma-Aldrich, St. Louis, USA) and Wheat Germ Agglutinin, Alexa FluorTM 647 conjugate (ThermoFisher Scientific) to highlight nuclei and plasma membrane. After 20 minutes, the sections were mounted using FluorsaveTM Reagent (Merck). The images were recorded using the Nanozoomer 2HT slide scanner (Hamamatsu) and analyzed using a homemade ImageJ plugin.

For electron microscopy, the muscles were fixed in 2.5% glutaraldehyde and 2.5% paraformaldehyde and 50 mM Ca^{2+} in cacodylate buffer (0.1 M, pH 7.4), washed in cacodylate buffer for 30 min, postfixed in 1% osmium tetroxide in 0.1M cacodylate buffer for 1 h at 4°C, and incubated with 5% uranyl acetate for 2 h at 4°C. The samples were dehydrated through graded alcohol (50, 70, 90, and 100%) and propylene oxide for 30 minutes each, and embedded in Epon 812. Semithin sections were cut at 2 μm on an Leica Ultracut microtome (Leica, Wetzlar, Germany) and contrasted with toluidine blue, and

ultrathin sections were cut at 70 nm and contrasted with uranyl acetate and lead citrate and examined at 70 kv with a Morgagni 268D electron microscope (FEI, [Electron Optics, Eindhoven, the Netherlands](#)). Images were captured digitally by Mega View III camera (Soft Imaging System, Münster, Germany).

Protein studies

Tibialis anterior, soleus, and gastrocnemius cryosections were lysed in radio immunoprecipitation (RIPA) buffer supplemented with 1 mM PMSF and complete mini EDTA-free protease inhibitor cocktail (Roche). Protein concentrations were determined using DCTM Protein Assay kit (BIO-RAD), and 10 µg of denatured protein samples in 5x Lane Marker Reducing Buffer (ThermoFisher Scientific) were loaded on a 10% SDS-PAGE gel containing 2,2,2-Trichloroethanol (TCE). The gel was then UV-activated for 45 s on a ChemiDocTM Touch Imaging System (BIO-RAD), and transferred to a nitrocellulose membrane for 7 min at 2.5 A using Transblot[®] TurboTM RTA Transfer Kit (BIO-RAD). Membranes were blocked for 1 hour in Tris-buffered saline (TBS) buffer containing 5% non-fat dry milk and 0.1% Tween 20. For immunofluorescence, tibialis anterior cryosections were fixed, and blocked with fetal calf serum. Following primary and secondary antibodies were used: rabbit anti-STIM1 (AB9870, Millipore, Burlington, USA), mouse anti-MHCI (BA-F8, DHSB, Iowa, USA), mouse anti MHCIIa (SC-71, DHSB), peroxidase-coupled goat anti-rabbit (112-036-062, Jackson ImmunoResearch, Ely, UK),. Images were recorded with the Amersham Imager 600 (Amersham, UK) and the DMRXA2 microscope (Leica).

Expression studies

RNA from tibialis anterior and soleus muscles was extracted with TRI Reagent (Molecular Research Center, Cincinnati, USA), and cDNA synthesis was performed using the SuperScriptTM II Transcriptase (ThermoFisher Scientific). For quantitative PCR, the cDNA

was amplified with SYBR Green Master Mix I (Roche) and 0.1 μ M forward and reverse interexonic primers (Supplemental Table S5), and amplicons were analyzed with a Lightcycler® 480 (Roche). Primers specificity was determined through a melting curve, and PCR products were Sanger-sequenced. Primer sequences for *Rpl27* were obtained from the literature (54). *Ca²⁺ measurements*

Primary myoblasts from 5 days old WT and *Stim1^{R304W/+}* mice were isolated as described before (55), and non-adherent cells were collected and plated in IMDM supplemented with 20% FCS and 1% CEE (chicken embryo extract) on Matrigel Reduced Factor-coated plates (Corning Life Sciences, Corning, USA). Cells were grown and transferred to laminin-coated ibidi (ibidi GmbH, Martinsried, Germany) or MatTek dishes (MatTek Corporation, Ashland, USA), and differentiated at 70% confluency. Experiments were carried out 4 days post differentiation

To quantify Ca^{2+} entry and Ca^{2+} store content, myotubes were incubated in Ringer solution containing 2 mM Ca^{2+} and 5 μ M Indo-1 or fura-2 for 30 min, washed, and incubated in 2 mM Ca^{2+} Ringer solution for another 30 min. The resting Ca^{2+} concentration was assessed in Fura-2 loaded myotubes as previously described (56). For Ca^{2+} entry, the medium was then replaced by Ca^{2+} -free Ringer solution, 10 mM Ca^{2+} was added after 5 min, and 25 mM caffeine after additional 2 min. For the Ca^{2+} store content, the medium was replaced by Ca^{2+} -free Ringer solution for 1 minute prior to addition of 10 mM caffeine and 1 μ M thapsigargin. The Ca^{2+} store content was calculated as the area under the curve between 50 and 300 seconds. The emission ratio of the Ca^{2+} indicator (405nm/485nm) was measured every 1.3 seconds on a SP8 UV confocal microscope (Leica). *Statistical analyses*

Data were verified for normal distribution using the Shapiro-Wilk test, and are presented as mean \pm SEM. For normally distributed data, significance of changes between WT and

Stim1^{R304W/+} mice of same gender was examined using a Student's t-test (with or without Welch's correction). For other data, a Mann-Whitney statistical test was performed. For the circularity and MinFerret distribution of fibers, the significance was assessed by two-way ANOVA followed by *post hoc* Bonferroni. Significant differences are illustrated as *(p<0.05), **(p<0.01), ***(p<0.001) and *****(p<0.0001).

Acknowledgements

We thank Michel Roux, Valerie Lalanne, Alexandru Parlog, Hamid Meziane, Aurelie Auburtin, Marie-Franche Champy, Josiane Hergueux, Thomas Harbonnier, Hamid Meziane, and Ghina Bou About for technical support. This work was funded by Fondation Maladies Rares (FMR) and Association Française contre les Myopathies (AFM-Telethon). Roberto Silva-Rojas was funded through a doctoral fellowship from Fondation Recherche Médicale (FRM, PLP20170939073).

Conflict of interest statement

None of the authors declares conflict of interest.

References

- 1 Lacruz, R.S. and Feske, S. (2015) Diseases caused by mutations in ORAI1 and STIM1. *Ann. N. Y. Acad. Sci.*, **1356**, 45-79.
- 2 Park, C.Y., Hoover, P.J., Mullins, F.M., Bachhawat, P., Covington, E.D., Raunser, S., Walz, T., Garcia, K.C., Dolmetsch, R.E. and Lewis, R.S. (2009) STIM1 clusters and activates CRAC channels via direct binding of a cytosolic domain to Orai1. *Cell*, **136**, 876-890.
- 3 Luik, R.M., Wu, M.M., Buchanan, J. and Lewis, R.S. (2006) The elementary unit of store-operated Ca²⁺ entry: local activation of CRAC channels by STIM1 at ER-plasma membrane junctions. *J. Cell Biol.*, **174**, 815-825.

- 4 Stathopoulos, P.B., Zheng, L., Li, G.Y., Plevin, M.J. and Ikura, M. (2008) Structural and mechanistic insights into STIM1-mediated initiation of store-operated calcium entry. *Cell*, **135**, 110-122.
- 5 Feske, S., Gwack, Y., Prakriya, M., Srikanth, S., Puppel, S.H., Tanasa, B., Hogan, P.G., Lewis, R.S., Daly, M. and Rao, A. (2006) A mutation in Orai1 causes immune deficiency by abrogating CRAC channel function. *Nature*, **441**, 179-185.
- 6 Picard, C., McCarl, C.A., Papolos, A., Khalil, S., Luthy, K., Hivroz, C., LeDeist, F., Rieux-Laucat, F., Rechavi, G., Rao, A. *et al.* (2009) STIM1 mutation associated with a syndrome of immunodeficiency and autoimmunity. *N. Engl. J. Med.*, **360**, 1971-1980.
- 7 Bohm, J., Chevessier, F., Maues De Paula, A., Koch, C., Attarian, S., Feger, C., Hantai, D., Laforet, P., Ghorab, K., Vallat, J.M. *et al.* (2013) Constitutive activation of the calcium sensor STIM1 causes tubular-aggregate myopathy. *Am. J. Hum. Genet.*, **92**, 271-278.
- 8 Misceo, D., Holmgren, A., Louch, W.E., Holme, P.A., Mizobuchi, M., Morales, R.J., De Paula, A.M., Stray-Pedersen, A., Lyle, R., Dalhus, B. *et al.* (2014) A dominant STIM1 mutation causes Stormorken syndrome. *Hum. Mutat.*, **35**, 556-564.
- 9 Morin, G., Bruechle, N.O., Singh, A.R., Knopp, C., Jedraszak, G., Elbracht, M., Bremond-Gignac, D., Hartmann, K., Sevestre, H., Deutz, P. *et al.* (2014) Gain-of-Function Mutation in STIM1 (P.R304W) Is Associated with Stormorken Syndrome. *Hum. Mutat.*, **35**, 1221-1232.
- 10 Nesin, V., Wiley, G., Kousi, M., Ong, E.C., Lehmann, T., Nicholl, D.J., Suri, M., Shahrizaila, N., Katsanis, N., Gaffney, P.M. *et al.* (2014) Activating mutations in STIM1 and ORAI1 cause overlapping syndromes of tubular myopathy and congenital miosis. *Proc. Natl. Acad. Sci. U. S. A.*, **111**, 4197-4202.

- 11 Chevessier, F., Bauche-Godard, S., Leroy, J.P., Koenig, J., Paturneau-Jouas, M., Eymard, B., Hantai, D. and Verdier-Sahuque, M. (2005) The origin of tubular aggregates in human myopathies. *J. Pathol.*, **207**, 313-323.
- 12 Bohm, J., Bulla, M., Urquhart, J.E., Malfatti, E., Williams, S.G., O'Sullivan, J., Szlauer, A., Koch, C., Baranello, G., Mora, M. *et al.* (2017) ORAI1 Mutations with Distinct Channel Gating Defects in Tubular Aggregate Myopathy. *Hum. Mutat.*, **38**, 426-438.
- 13 Endo, Y., Noguchi, S., Hara, Y., Hayashi, Y.K., Motomura, K., Miyatake, S., Murakami, N., Tanaka, S., Yamashita, S., Kizu, R. *et al.* (2015) Dominant mutations in ORAI1 cause tubular aggregate myopathy with hypocalcemia via constitutive activation of store-operated Ca(2)(+) channels. *Hum. Mol. Genet.*, **24**, 637-648.
- 14 Markello, T., Chen, D., Kwan, J.Y., Horkayne-Szakaly, I., Morrison, A., Simakova, O., Maric, I., Lozier, J., Cullinane, A.R., Kilo, T. *et al.* (2015) York platelet syndrome is a CRAC channelopathy due to gain-of-function mutations in STIM1. *Mol. Genet. Metab.*, **114**, 474-482.
- 15 Noury, J.B., Bohm, J., Peche, G.A., Guyant-Marechal, L., Bedat-Millet, A.L., Chiche, L., Carlier, R.Y., Malfatti, E., Romero, N.B. and Stojkovic, T. (2017) Tubular aggregate myopathy with features of Stormorken disease due to a new STIM1 mutation. *Neuromuscul. Disord.*, **27**, 78-82.
- 16 Walter, M.C., Rossius, M., Zitzelsberger, M., Vorgerd, M., Muller-Felber, W., Ertl-Wagner, B., Zhang, Y., Brinkmeier, H., Senderek, J. and Schoser, B. (2015) 50 years to diagnosis: Autosomal dominant tubular aggregate myopathy caused by a novel STIM1 mutation. *Neuromuscul. Disord.*, **25**, 577-584.
- 17 Garibaldi, M., Fattori, F., Riva, B., Labasse, C., Brochier, G., Ottaviani, P., Sacconi, S., Vizzaccaro, E., Laschena, F., Romero, N.B. *et al.* (2017) A novel gain-of-function

mutation in ORAI1 causes late-onset tubular aggregate myopathy and congenital miosis. *Clin. Genet.*, **91**, 780-786.

18 Bohm, J. and Laporte, J. (2018) Gain-of-function mutations in STIM1 and ORAI1 causing tubular aggregate myopathy and Stormorken syndrome. *Cell Calcium*, **76**, 1-9.

19 Harris, E., Burki, U., Marini-Bettolo, C., Neri, M., Scotton, C., Hudson, J., Bertoli, M., Evangelista, T., Vroiling, B., Polvikoski, T. *et al.* (2017) Complex phenotypes associated with STIM1 mutations in both coiled coil and EF-hand domains. *Neuromuscul. Disord.*, **27**, 861-872.

20 Alonso-Jimenez, A., Ramon, C., Dols-Icardo, O., Roig, C., Gallardo, E., Clarimon, J., Nunez-Peralta, C. and Diaz-Manera, J. (2018) Corpus callosum agenesis, myopathy and pinpoint pupils: consider Stormorken syndrome. *Eur. J. Neurol.*, **25**, e25-e26.

21 Fahrner, M., Stadlbauer, M., Muik, M., Rathner, P., Stathopoulos, P., Ikura, M., Muller, N. and Romanin, C. (2018) A dual mechanism promotes switching of the Stormorken STIM1 R304W mutant into the activated state. *Nat. Commun.*, **9**, 825.

22 Braun, A., Varga-Szabo, D., Kleinschnitz, C., Pleines, I., Bender, M., Austinat, M., Bosl, M., Stoll, G. and Nieswandt, B. (2009) Orai1 (CRACM1) is the platelet SOC channel and essential for pathological thrombus formation. *Blood*, **113**, 2056-2063.

23 Varga-Szabo, D., Braun, A., Kleinschnitz, C., Bender, M., Pleines, I., Pham, M., Renne, T., Stoll, G. and Nieswandt, B. (2008) The calcium sensor STIM1 is an essential mediator of arterial thrombosis and ischemic brain infarction. *J. Exp. Med.*, **205**, 1583-1591.

24 Stiber, J., Hawkins, A., Zhang, Z.S., Wang, S., Burch, J., Graham, V., Ward, C.C., Seth, M., Finch, E., Malouf, N. *et al.* (2008) STIM1 signalling controls store-operated calcium entry required for development and contractile function in skeletal muscle. *Nat. Cell Biol.*, **10**, 688-697.

- 25 McCarl, C.A., Khalil, S., Ma, J., Oh-hora, M., Yamashita, M., Roether, J., Kawasaki, T., Jairaman, A., Sasaki, Y., Prakriya, M. *et al.* (2010) Store-operated Ca²⁺ entry through ORAI1 is critical for T cell-mediated autoimmunity and allograft rejection. *J. Immunol.*, **185**, 5845-5858.
- 26 Oh-Hora, M., Yamashita, M., Hogan, P.G., Sharma, S., Lamperti, E., Chung, W., Prakriya, M., Feske, S. and Rao, A. (2008) Dual functions for the endoplasmic reticulum calcium sensors STIM1 and STIM2 in T cell activation and tolerance. *Nat. Immunol.*, **9**, 432-443.
- 27 Ahmad, F., Boulaftali, Y., Greene, T.K., Ouellette, T.D., Poncz, M., Feske, S. and Bergmeier, W. (2011) Relative contributions of stromal interaction molecule 1 and CalDAG-GEFI to calcium-dependent platelet activation and thrombosis. *J. Thromb. Haemost.*, **9**, 2077-2086.
- 28 Grosse, J., Braun, A., Varga-Szabo, D., Beyersdorf, N., Schneider, B., Zeitlmann, L., Hanke, P., Schropp, P., Muhlstedt, S., Zorn, C. *et al.* (2007) An EF hand mutation in Stim1 causes premature platelet activation and bleeding in mice. *J. Clin. Invest.*, **117**, 3540-3550.
- 29 Stormorken, H., Sjaastad, O., Langslet, A., Sulg, I., Egge, K. and Diderichsen, J. (1985) A new syndrome: thrombocytopathia, muscle fatigue, asplenia, miosis, migraine, dyslexia and ichthyosis. *Clin. Genet.*, **28**, 367-374.
- 30 Chevessier, F., Marty, I., Paturneau-Jouas, M., Hantai, D. and Verdiere-Sahuque, M. (2004) Tubular aggregates are from whole sarcoplasmic reticulum origin: alterations in calcium binding protein expression in mouse skeletal muscle during aging. *Neuromuscul. Disord.*, **14**, 208-216.
- 31 Bohm, J., Chevessier, F., Koch, C., Peche, G.A., Mora, M., Morandi, L., Pasanisi, B., Moroni, I., Tasca, G., Fattori, F. *et al.* (2014) Clinical, histological and genetic

characterisation of patients with tubular aggregate myopathy caused by mutations in STIM1. *Journal of medical genetics*, **51**, 824-833.

32 Bohm, J., Lornage, X., Chevessier, F., Birck, C., Zanotti, S., Cudia, P., Bulla, M., Granger, F., Bui, M.T., Sartori, M. *et al.* (2018) CASQ1 mutations impair calsequestrin polymerization and cause tubular aggregate myopathy. *Acta Neuropathol.*, **135**, 149-151.

33 Hedberg, C., Niceta, M., Fattori, F., Lindvall, B., Ciolfi, A., D'Amico, A., Tasca, G., Petrini, S., Tulinius, M., Tartaglia, M. *et al.* (2014) Childhood onset tubular aggregate myopathy associated with de novo STIM1 mutations. *J. Neurol.*, **261**, 870-876.

34 Arruda, A.P., Pers, B.M., Parlakgul, G., Guney, E., Goh, T., Cagampan, E., Lee, G.Y., Goncalves, R.L. and Hotamisligil, G.S. (2017) Defective STIM-mediated store operated Ca(2+) entry in hepatocytes leads to metabolic dysfunction in obesity. *Elife*, **6**.

35 Kono, T., Tong, X., Taleb, S., Bone, R.N., Iida, H., Lee, C.C., Sohn, P., Gilon, P., Roe, M.W. and Evans-Molina, C. (2018) Impaired Store-Operated Calcium Entry and STIM1 Loss Lead to Reduced Insulin Secretion and Increased Endoplasmic Reticulum Stress in the Diabetic beta-Cell. *Diabetes*, **67**, 2293-2304.

36 Schiaffino, S. and Reggiani, C. (2011) Fiber types in mammalian skeletal muscles. *Physiological reviews*, **91**, 1447-1531.

37 Parekh, A.B. and Penner, R. (1997) Store depletion and calcium influx. *Physiol. Rev.*, **77**, 901-930.

38 Shahrizaila, N., Lowe, J. and Wills, A. (2004) Familial myopathy with tubular aggregates associated with abnormal pupils. *Neurology*, **63**, 1111-1113.

39 Bodensteiner, J.B. and Engel, A.G. (1978) Intracellular calcium accumulation in Duchenne dystrophy and other myopathies: a study of 567,000 muscle fibers in 114 biopsies. *Neurology*, **28**, 439-446.

- 40 Perry, R.L. and Rudnick, M.A. (2000) Molecular mechanisms regulating myogenic determination and differentiation. *Front. Biosci.*, **5**, D750-767.
- 41 Agbulut, O., Destombes, J., Thiesson, D. and Butler-Browne, G. (2000) Age-related appearance of tubular aggregates in the skeletal muscle of almost all male inbred mice. *Histochem. Cell. Biol.*, **114**, 477-481.
- 42 Ekiz, O., Balta, I., Sen, B.B., Rifaioglu, E.N., Ergin, C., Balta, S. and Demirkol, S. (2014) Mean platelet volume in recurrent aphthous stomatitis and Behcet disease. *Angiology*, **65**, 161-165.
- 43 Soydinc, S., Turkbeyler, I.H., Pehlivan, Y., Soylu, G., Goktepe, M.F., Bilici, M., Zengin, O., Kisacik, B. and Onat, A.M. (2014) Mean platelet volume seems to be a valuable marker in patients with systemic sclerosis. *Inflammation*, **37**, 100-106.
- 44 Wang, X., Meng, H., Xu, L., Chen, Z., Shi, D. and Lv, D. (2015) Mean platelet volume as an inflammatory marker in patients with severe periodontitis. *Platelets*, **26**, 67-71.
- 45 Noack, M. and Miossec, P. (2014) Th17 and regulatory T cell balance in autoimmune and inflammatory diseases. *Autoimmun. Rev.*, **13**, 668-677.
- 46 Hwang, S.Y. and Putney, J.W. (2012) Orai1-mediated calcium entry plays a critical role in osteoclast differentiation and function by regulating activation of the transcription factor NFATc1. *FASEB J.*, **26**, 1484-1492.
- 47 Robinson, L.J., Mancarella, S., Songsawad, D., Tourkova, I.L., Barnett, J.B., Gill, D.L., Soboloff, J. and Blair, H.C. (2012) Gene disruption of the calcium channel Orai1 results in inhibition of osteoclast and osteoblast differentiation and impairs skeletal development. *Lab Invest.*, **92**, 1071-1083.
- 48 Byun, M., Abhyankar, A., Lelarge, V., Plancoulaine, S., Palanduz, A., Telhan, L., Boisson, B., Picard, C., Dewell, S., Zhao, C. *et al.* (2010) Whole-exome sequencing-based

discovery of STIM1 deficiency in a child with fatal classic Kaposi sarcoma. *J. Exp. Med.*, **207**, 2307-2312.

49 Fuchs, S., Rensing-Ehl, A., Speckmann, C., Bengsch, B., Schmitt-Graeff, A., Bondzio, I., Maul-Pavicic, A., Bass, T., Vraetz, T., Strahm, B. *et al.* (2012) Antiviral and regulatory T cell immunity in a patient with stromal interaction molecule 1 deficiency. *J. Immunol.*, **188**, 1523-1533.

50 McCarl, C.A., Picard, C., Khalil, S., Kawasaki, T., Rother, J., Papolos, A., Kutok, J., Hivroz, C., Ledest, F., Plogmann, K. *et al.* (2009) ORAI1 deficiency and lack of store-operated Ca²⁺ entry cause immunodeficiency, myopathy, and ectodermal dysplasia. *J. Allergy Clin. Immunol.*, **124**, 1311-1318 e1317.

51 Chou, J., Badran, Y.R., Yee, C.S., Bainter, W., Ohsumi, T.K., Al-Hammadi, S., Pai, S.Y., Feske, S. and Geha, R.S. (2015) A novel mutation in ORAI1 presenting with combined immunodeficiency and residual T-cell function. *J. Allergy Clin. Immunol.*, **136**, 479-482 e471.

52 Schaballie, H., Rodriguez, R., Martin, E., Moens, L., Frans, G., Lenoir, C., Dutre, J., Canioni, D., Bossuyt, X., Fischer, A. *et al.* (2015) A novel hypomorphic mutation in STIM1 results in a late-onset immunodeficiency. *J. Allergy Clin. Immunol.*, **136**, 816-819 e814.

53 Wang, S., Choi, M., Richardson, A.S., Reid, B.M., Seymen, F., Yildirim, M., Tuna, E., Gencay, K., Simmer, J.P. and Hu, J.C. (2014) STIM1 and SLC24A4 Are Critical for Enamel Maturation. *J. Dent. Res.*, **93**, 94S-100S.

54 Thomas, K.C., Zheng, X.F., Garces Suarez, F., Raftery, J.M., Quinlan, K.G., Yang, N., North, K.N. and Houweling, P.J. (2014) Evidence based selection of commonly used RT-qPCR reference genes for the analysis of mouse skeletal muscle. *PLoS One*, **9**, e88653.

55 De Palma, S., Capitanio, D., Vasso, M., Braghetta, P., Scotton, C., Bonaldo, P., Lochmuller, H., Muntoni, F., Ferlini, A. and Gelfi, C. (2014) Muscle proteomics reveals

novel insights into the pathophysiological mechanisms of collagen VI myopathies. *J. Proteome Res.*, **13**, 5022-5030.

56 Bachmann, C., Jungbluth, H., Muntoni, F., Manzur, A.Y., Zorzato, F. and Treves, S. (2017) Cellular, biochemical and molecular changes in muscles from patients with X-linked myotubular myopathy due to MTM1 mutations. *Hum. Mol. Genet.*, **26**, 320-332.

Figure legends

Figure 1. *Stim1*^{R304W/+} mice manifested a multi-systemic phenotype. (A) Survival rate shows a decrease of 50% for *Stim1*^{R304W/+} mice at 9 months (n=9-11). (B, C) At 4 months, whole-body weight and size of *Stim1*^{R304W/+} mice were significantly reduced compared to controls. (D) 3D representations illustrating the abnormal trabecular microarchitecture (in pink) in the distal femur of 4 months old *Stim1*^{R304W/+} mice. (E) Spleen enlargement was evident in 4 months old *Stim1*^{R304W/+} mice, while heart, brain, and liver weight were normal (n=3-19). (F) Relative muscle weight at 4 months revealed hypertrophy of the soleus and hypotrophy of the gastrocnemius from *Stim1*^{R304W/+} mice, while EDL and tibialis anterior (TA) were comparable to the controls (n=6-14). (G) Representative pupil orientation at 4 months showed upward gaze paresis in *Stim1*^{R304W/+} mice. (H, I) Blood counts revealed a reduced platelet number and an increased mean platelet volume in *Stim1*^{R304W/+} mice.

Figure 1

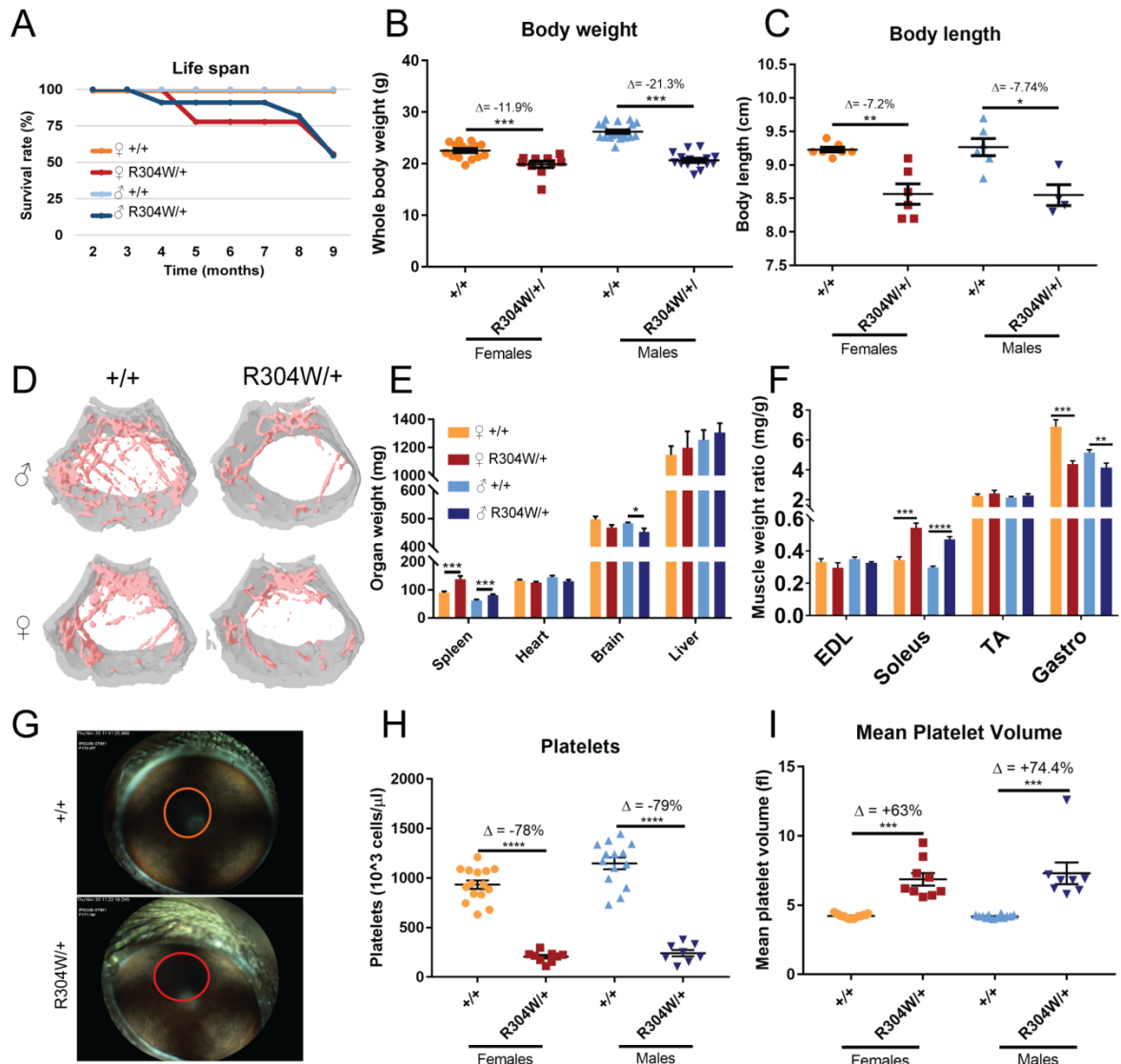


Figure 2. Abnormal immune system in *Stim1*^{R304W/+} mice. (A, B) Blood counts at 4 months disclosed increased neutrophils and monocytes, and decreased lymphocytes *Stim1*^{R304W/+} mice compared to controls (n=8-15). (C) H&E staining on spleen sections revealed megakaryocyte hyperplasia (dark arrows) in *Stim1*^{R304W/+} mice at 4 months. (D) Compared to controls, regulatory T cells (Treg) and nuclear killer cells (NKc) were decreased in *Stim1*^{R304W/+} spleen at 4 months (n=5).

Figure 2

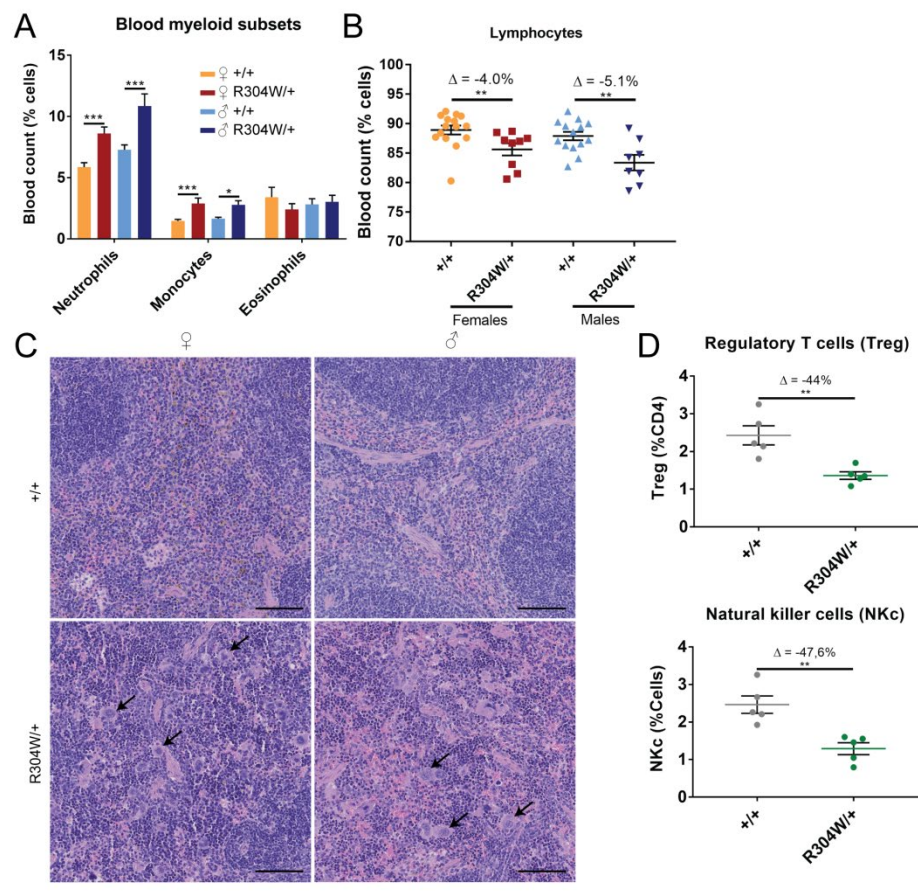


Figure 3. *Stim1*^{R304W/+} mice produced less force and exhibited delayed muscle relaxation.

(A) The open field test at 9 weeks of age revealed a reduction in speed and covered distance for *Stim1*^{R304W/+} mice compared to WT controls. (B) The Rotarod test at 9 weeks of age did not reveal coordination differences between *Stim1*^{R304W/+} and WT mice. (C, D) *Stim1*^{R304W/+} mice had less grip strength and showed reduced hanging time compared to controls. (E) Tibialis anterior (TA) force measurements at 9 months (left) and representative traces revealed reduced specific force of *Stim1*^{R304W/+} males, while *Stim1*^{R304W/+} females were comparable to controls. Both *Stim1*^{R304W/+} males and females showed a delay in force decrease subsequent to stimulation (right). (F) At 9 months, *Stim1*^{R304W/+} tibialis anterior exhibited an increased time to fatigue upon continuous stimulation (left). Representative traces over 20 s illustrate the slower force decrease of *Stim1*^{R304W/+} mice compared to controls (middle and right).

Figure 3

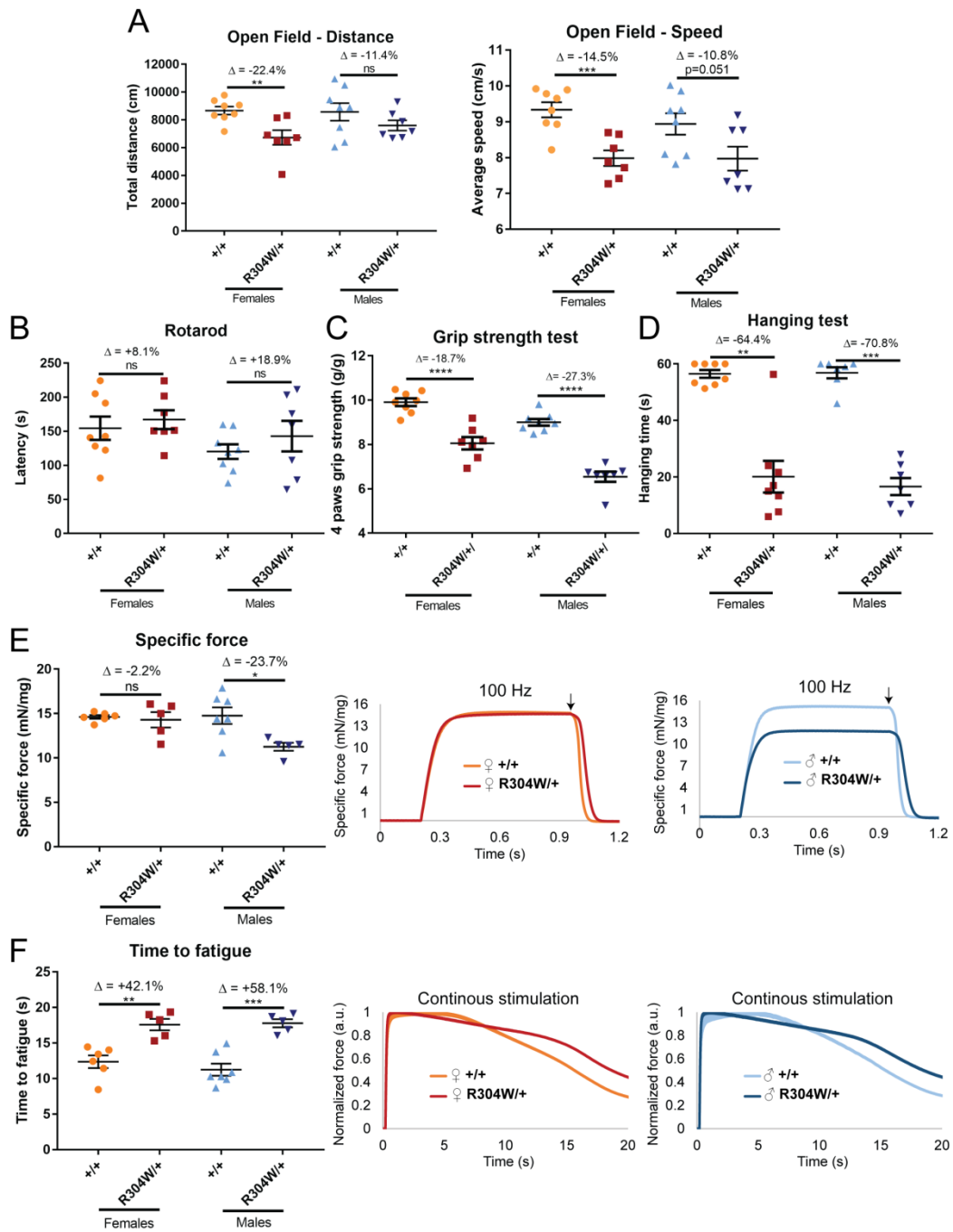


Figure 4. *Stim1*^{R304W/+} muscle histology showed dystrophic features, but no tubular aggregates. (A) H&E, Gomori trichrome, ATPase, and Alizarin red staining of transverse tibialis anterior sections at 4 months revealed internalized nuclei (green arrow), regenerating fibers (blue arrow), infiltration of inflammatory cells (red arrow), fibrosis (pink arrow), higher proportion of dark type I fibers, and rounded fibers with intense Ca²⁺ signals (black arrows) in *Stim1*^{R304W/+} mice (scale bar = 50 μm). (B) MinFerret distribution showed a reduced proportion of large fibers (> 50 μm) in *Stim1*^{R304W/+} tibialis anterior at 4 months (n=4, 1900 fibers/mice in average). (C) Circularity distribution revealed a higher proportion of rounded tibialis anterior fibers in *Stim1*^{R304W/+} mice at 4 months. Circularity ranges from 0 a.u. (line) to 1 a.u. (circle). (D) Electron microscopy on longitudinal (left) and transversal (right) TA sections at 9 months revealed swollen mitochondria in *Stim1*^{R304W/+} mice (scale bar = 2 μm).

Figure 4

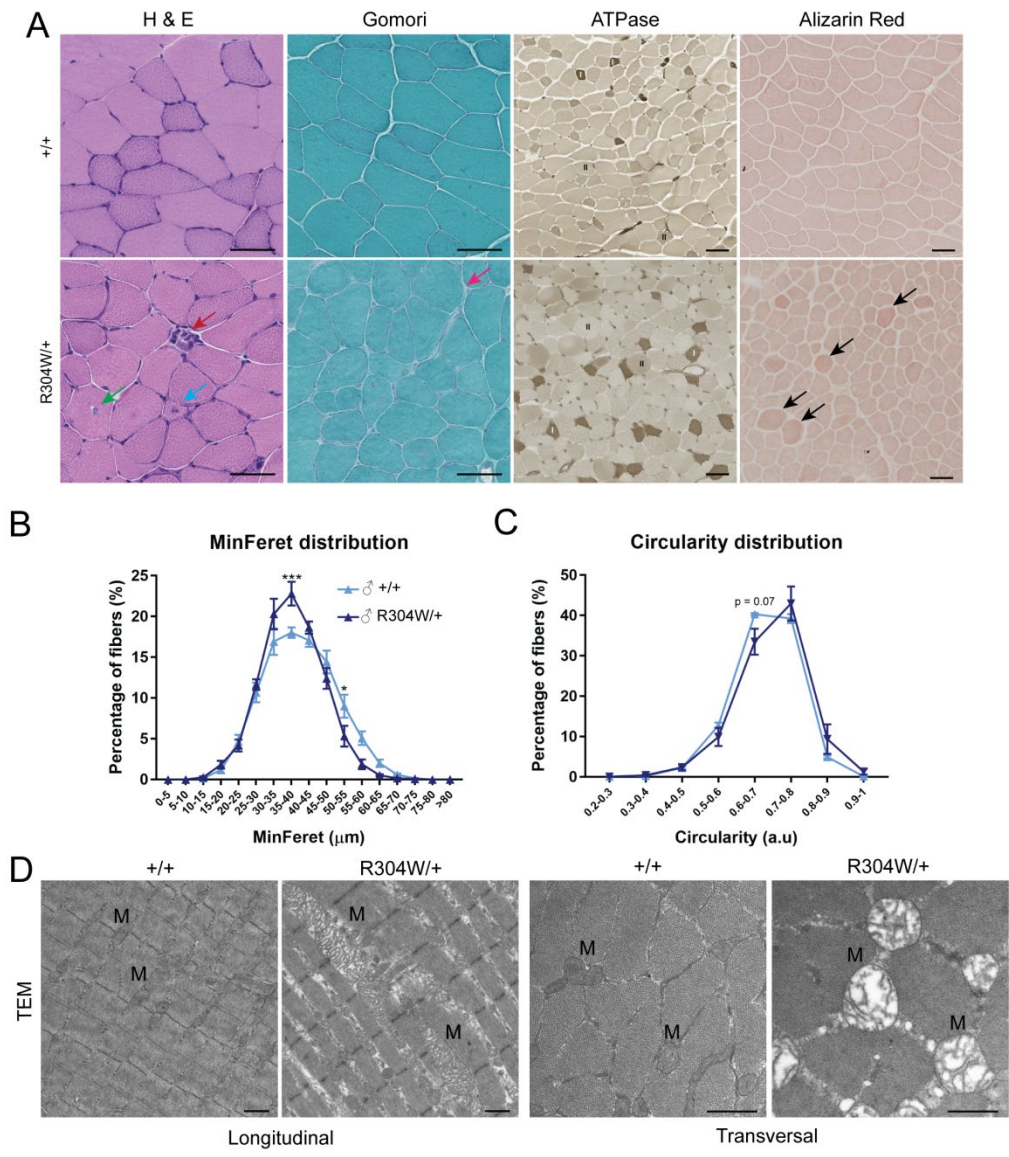


Figure 5. Abnormal Ca²⁺ homeostasis in *Stim1*^{R304W/+} mice (A) Blood analyses revealed hypocalcemia and hyperphosphatemia in *Stim1*^{R304W/+} mice at 4 months (n=6-15). (B) Ca²⁺ measurements revealed increased resting Ca²⁺ in differentiated myotubes from *Stim1*^{R304W/+} mice compared to controls (left, n=51-57 from 5-6 mice per genotype). (C) Mean normalized Indo-1 ratio measurements over time demonstrated an increased extracellular Ca²⁺ entry in *Stim1*^{R304W/+} myotubes upon addition of 10 mM Ca²⁺ to the medium. Subsequent addition of caffeine confirmed the differentiation state of the myotubes (left, n=27-29 from 5-6 mice per genotype). (D) SOCE amplitude, representing the maximal Indo-1 ratio following addition of Ca²⁺, was increased in *Stim1*^{R304W/+} myotubes compared to WT controls (right, n=27-29 from 5-6 mice per genotype). The basal Indo-1 fluorescence of the *Stim1*^{R304W/+} myotubes were normalized to the WT level to highlight the relative differences in SOCE amplitude. (E) Logarithmic illustration of gene expression shows downregulation of the Ca²⁺ regulators *Stim1* and *Casq1* and upregulation of the NFAT target genes *Myog* and *Myf5* in *Stim1*^{R304W/+} tibialis anterior at 4 months compared to controls (n=5).

Figure 5

